Chemical Science

Cite this: *Chem. Sci.*, 2012, **3**, 2330

www.rsc.org/chemicalscience

EDGE ARTICLE

Layered manganese oxides for water-oxidation: alkaline earth cations influence catalytic activity in a photosystem II-like fashion†

Mathias Wiechen,[a] Ivelina Zaharieva,[b] Holger Dau*[b] and Philipp Kurz*[a]

Received 23rd February 2012, Accepted 17th April 2012
DOI: 10.1039/c2sc20226c

In reaction sequences for light driven water-splitting into H_2 and O_2, water-oxidation is a crucial reaction step. *In vivo*, the process is catalysed within a photoenzyme called photosystem II (PSII) by a μ-oxido $CaMn_4$ cluster, the oxygen-evolving complex (OEC). The OEC is known to be virtually inactive if Ca^{2+} is removed from its structure. Activity can be restored not only by the addition of Ca^{2+} but also Sr^{2+} ions. We have recently introduced layered calcium manganese oxides of the birnessite mineral family as functional synthetic model compounds for the OEC. Here, we present the syntheses of layered manganese oxides where we varied the interlayer cations, preparing a series of K-, Ca-, Sr- and Mg-containing birnessites. Structural motifs within these materials were determined using X-ray absorption spectroscopy (XAS) showing that all materials have similar atomic structures despite their different elemental compositions. Water-oxidation experiments were carried out to elucidate structure-reactivity relations. These experiments demonstrated that the oxides—like the OEC—require the presence of calcium in their structures to reach maximum catalytic activity. As another similarity to the OEC, Sr^{2+} is the "second best choice" for the secondary cation. The results thus support mechanistic proposals which involve an important catalytic role for Ca^{2+} in biological water-oxidation. Additionally, they offer valuable hints for the development of synthetic, manganese-based water-oxidation catalysts for artificial photosynthesis.

Introduction

In the broad field of research on alternative energy production, light-driven water splitting into H_2 and O_2 is an intensely discussed approach.[1–7] One of the biggest challenges here is the development of efficient and affordable transition-metal based catalysts for the four-electron oxidation of water to molecular oxygen (eqn (1)) for which especially compounds containing Co-, Ir-, Mn- and Ru-active sites have been extensively studied.[4–17]

$$2H_2O \rightarrow O_2 + 4\,H^+ + 4\,e^- \quad (1)$$

In nature, water-oxidation is catalysed within photosystem II (PSII), a transmembrane cofactor-protein complex embedded in the thylakoid membranes of plants and cyanobacteria. In PSII, the active site for water-oxidation is formed by the oxygen-evolving complex (OEC, or water-oxidising complex, WOC).[4,18–20] The OEC is a highly active water-oxidation catalyst built up from abundant elements. Therefore a number of researchers, including us, see the OEC as a possible blueprint for the development of affordable synthetic catalysts for reaction (1).[9,11,21–24]

A crystal structure of PSII at a resolution of 1.9 Å was recently published by Umena *et al.*, showing the structure of the OEC to be a $CaMn_4O_5$ complex closely bound to its highly conserved amino acid environment.[25] The metal ions are interconnected by μ-oxido ligands, with three Mn and one Ca forming a distorted $CaMn_3O_4$ cubane. The fourth manganese ion is then bound to this moiety by additional μ-oxido ligands. This new structural information represents an enormous progress in PSII research. However, the exact mechanism of water-oxidation catalysis by the OEC is still not known. Nevertheless, it is clear today that the $CaMn_4O_5$ complex is oxidised stepwise in single-electron steps during the water-oxidation reaction, cycling through five individual oxidation states. Oxidizing equivalents are stored in the $CaMn_4O_5$ complex mainly through Mn-centred oxidations as the manganese ions are oxidized from Mn^{III} to Mn^{IV}.[26–29] For the highest oxidation state of the OEC (known as S_4), the oxidation of an oxido ligand (O^{-II}) to its oxyl radical form (O^{-I}) has been suggested.[30]

In addition to the Mn centres, Ca^{2+} plays a key role for the catalytic activity of the OEC.[31–36] It has been shown by several

[a]*Institut für Anorganische Chemie, Christian-Albrechts-Universität zu Kiel, 24118 Kiel, Germany. E-mail: phkurz@ac.uni-kiel.de; Fax: +49 431 880 1520; Tel: +49 431 880 5803*
[b]*Fachbereich Physik, Freie Universität Berlin, Arnimallee 14, 14195 Berlin, Germany. E-mail: holger.dau@fu-berlin.de; Fax: +49 30 838 56299; Tel: +49 30 838 53581*

† Electronic supplementary information (ESI) available: details concerning syntheses, characterisation methods, XAS measurements, EXAFS simulations, experiments on water-oxidation catalysis as well as additional figures and tables mentioned in the text. See DOI: 10.1039/c2sc20226c

research teams that water-oxidation catalysis by PSII is inhibited if calcium is removed from the protein. The activity of the Ca^{2+}-depleted enzyme can be restored not only by the addition of Ca^{2+}, but also (though to a lesser degree) by Sr^{2+} ions.[31–33,37] On the contrary, the addition of Mg^{2+} ions does not result in the recovery of activity.[31,33] Even though the absolute numbers for the catalytic rates of these cation-exchanged forms of PSII differ from one experimental protocol to the other, an "activity ranking" $Ca^{2+} > Sr^{2+} \gg Mg^{2+} \sim Na^{+}$ is by now clearly established.

Concerning the function of calcium for catalysis, Cox *et al.* recently demonstrated an analysis of EPR/ENDOR data and theoretical calculations and concluded that the substitution of Ca^{2+} by Sr^{2+} within PSII does not change the electronic structure of the OEC significantly.[38] Because Sr^{2+}-substituted PSII nevertheless shows much reduced activity, the authors concluded that it is unlikely that Ca^{2+} plays only a structural role in the OEC.[38] Rather, Ca^{2+} seems to be actively involved in the biological catalytic process, most probably either as a site for the binding and activation of water[25,39–43] or as a factor supporting S-state advancement.[42,43]

Inspired by the composition of the OEC and the fundamental role of Ca^{2+} for catalysis, we have synthesised and studied calcium-manganese oxides as bioinspired water-oxidation catalysts. These materials showed good catalytic activity in chemical water-oxidation experiments using both chemical and photochemical oxidation agents.[44]

Further research addressing the structures of the oxides by X-ray absorption spectroscopy (XAS) led us to the conclusion that these catalytically active manganese oxides are phyllomanganates composed of layers of edge-sharing MnO_6 octahedra analogous to naturally occurring minerals of the birnessite family.[45] As typical for birnessites, the average Mn oxidation state in these oxides was found to be around +3.8. The MnO_6-layers are highly disordered, containing a large number of Mn vacancies. In addition, intercalated Ca^{2+} ions could be identified in positions between the MnO_6-layers on top of vacancies in the layers. They could also be located in more ordered sections of the layers where they are then part of distorted complete or incomplete $CaMn_{2/3}(\mu\text{-}O)_4$ cubes.

The OEC is of course not a phyllomanganate. Nevertheless, synthetic birnessites are very similar to the active site for water-oxidation in PSII if parameters like the Mn–Mn-distances, the Mn oxidation states or the Mn–Mn/Mn–Ca connectivities are compared. The results of our structural studies thus indicated that synthetic calcium birnessites can be considered as very good mimics for key building units of the OEC. Additionally, they show promising catalytic activity in water-oxidation, which makes them interesting candidates for a possible application in water-splitting as part of alternative energy conversion systems.[9,45]

Other recent publications on birnessites have confirmed the potential of these materials to act as water-oxidation catalysts. For example, Hocking *et al.* identified birnessite nanoparticles originating from the decomposition of a tetranuclear manganese complex within a Nafion polymer matrix as the active species of a water-oxidation catalyst.[46] Pinaud *et al.* studied parameters like the electronic band structure and optical characteristics of Na-birnessite thin films in the context of electrochemical water-splitting.[47] Furthermore and independently to our studies, Mn-motifs similar to the ones described by us[45] were suggested to play a key role in water-oxidation catalysis.[48,49] And finally it has to be noted that the suitability of oxides with layered structures for water-oxidation catalysis is not limited to manganese: layered Co-[50,51] or Ni-oxides[52] featuring oxide structures similar to birnessites have by now also been reported to be highly active in catalysing reaction (1).[13,53]

Here, we now present important variations of the birnessite theme. We synthesised different layered manganese oxides containing not only Ca^{2+} but also K^{+}, Sr^{2+} or Mg^{2+} in different concentrations and investigated whether the variation of these secondary cations changed the catalytic activity of the oxides. The results have implications both as bioinorganic models for the OEC and for the development of synthetic catalysts for the water-oxidation reaction.

Results and discussion

Synthesis and characterisation of K/Ca/Sr/Mg-birnessites

Following previously established routes,[55] the birnessites for this study were prepared by comproportionation reactions of Mn^{2+} and MnO_4^- in the presence of the different alkali and alkaline earth cations at high pH (Scheme 1, see ESI† for details). Due to the very high affinity of MnO_6-layers for divalent cations,[56] it is possible to incorporate large amounts of alkali earth ions in the materials even if 10–100 times higher concentrations of Na^{+} or K^{+} are present in the reaction mixture. The original products obtained from the precipitation reactions after three days of ripening are most likely buserites,[54] which are phyllomanganates similar in their structures to birnessites. However, they contain larger amounts of intercalated water resulting in interlayer distances of 10 Å. These solids were not isolated as they are only stable as aqueous suspensions. Instead, we transformed the buserites into the corresponding stable birnessites **1–7** by drying in air at mild temperatures of 65 °C (Scheme 1).

The composition of the different synthesised oxides was analysed by energy-dispersive X-ray spectroscopy (see Table 1), atomic absorption spectroscopy (see ESI†, Table S2) and thermogravimetry (see Table 1, Fig. 1). We found that the oxides can be best formulated as $K_{0.31}$- (**1**), $Ca_{0.14}$- (**2**), $Ca_{0.27}$- (**3**), $Sr_{0.18}$- (**4**), $Sr_{0.27}$- (**5**), $Mg_{0.13}$- (**6**) and $Mg_{0.28}$-birnessites (**7**), where the

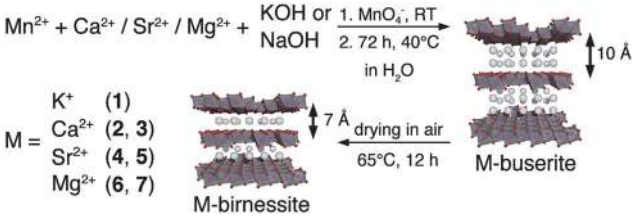

Scheme 1 Synthetic route for the preparation of K- (**1**), Ca- (**2**, **3**), Sr- (**4**, **5**) and Mg-birnessites (**6**, **7**). By variation of the initial metal ion concentrations, materials of different M : Mn ratios can be synthesised. The comproportionation reactions of Mn^{2+} and MnO_4^- under alkaline conditions initially result in the formation of metastable M-buserite intermediates,[54] which contain two layers of water (white spheres) in between the Mn-oxide layers. By drying at mild temperatures, one layer of water is removed and different M-birnessites can be isolated.[54]

Table 1 Atomic ratios (per Mn) and water content (in weight %) of the synthesised M-birnessites determined by EDX and DTG

Compound[a]	Na/K[b]	Mg	Ca	Sr	Mn	M : Mn	H_2O[c]
$K_{0.31}$ (**1**)	0.31	—	0.02	—	1	0.33	10
$Ca_{0.14}$ (**2**)	0.05*	—	0.14	—	1	0.19	15
$Ca_{0.27}$ (**3**)	0.03	—	0.27	—	1	0.30	18
$Sr_{0.18}$ (**4**)	0.08	—	—	0.18	1	0.26	12
$Sr_{0.27}$ (**5**)	0.01	—	—	0.27	1	0.28	11
$Mg_{0.13}$ (**6**)	0.19*	0.13	—	—	1	0.32	13
$Mg_{0.28}$ (**7**)	0.17	0.28	—	—	1	0.45	14

[a] The synthesised M-birnessites are labelled according to the additional cation that is primarily intercalated in between the manganese oxide layers. Indices describe the M : Mn molar ratio for the major cation. [b] Na (*) or K originating from the hydroxide bases used for the syntheses. [c] The recorded weight loss up to 400 °C was assumed to originate entirely from the elimination of water from the materials.

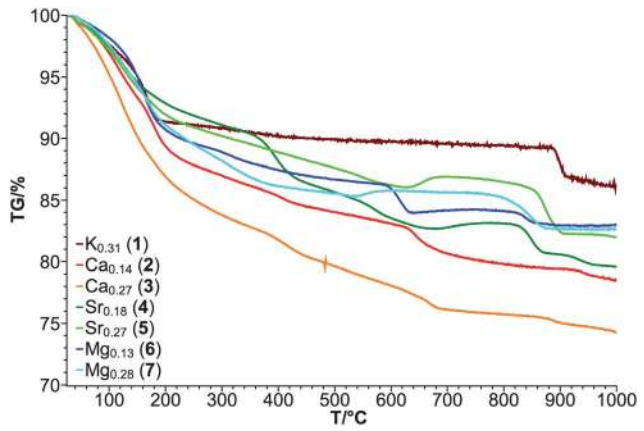

Fig. 1 Thermogravimetric analyses of M-birnessites **1–7**. Samples were heated to 1000 °C at a rate of 4 °C min^{-1} in air. The observed weight loss in the temperature range from 25 °C to about 400 °C is most probably caused by the loss of water. At higher temperatures, phase transitions coupled to oxygen release are likely to occur.[57]

indices represent the M : Mn molar ratio for M = K^+, Ca^{2+}, Sr^{2+} or Mg^{2+}. Oxide **1** was prepared under conditions virtually free of M^{2+} ions and thus served as a reference material representing a birnessite free of alkaline earth metals. If only small amounts of M^{2+} ions are present we observed that more sodium or potassium cations (originating from the hydroxide bases used for the synthesis) are incorporated into the material instead of the otherwise preferred divalent cations (see Table 1). Increased Na^+/K^+ contents were also observed for oxides containing the rather weakly binding Mg^{2+} as alkaline earth component. Strikingly, the ratio of the total amount of additional $M^{+/2+}$ ions per Mn ion is rather constant for most synthesised oxides of the series with M : Mn ratios of ~0.3 (see Table 1).

Thermogravimetric analyses of compounds **1–7** show weight losses of 10–20% in the temperature range from 25 °C to 400 °C (Fig. 1). These can most likely be explained by the loss of water weakly bound to the oxide layers (see Table 1 and Scheme 1). In the temperature range up to 1000 °C, the total weight is further reduced by about 15–30% (Fig. 1). For such higher temperatures it is known for binary manganese oxides like MnO_2 that phase transitions coupled to oxygen release occur, resulting in a stepwise reduction of manganese from Mn^{IV} *via* Mn^{III} to Mn^{II}.[57] As the synthetic birnessites studied here are compounds with a manganese oxidation state close to +IV (see XAS results, Table 1), similar events seem likely to occur here as well. The thermogravimetric data thus supports our identification of the materials as water-containing $Mn^{III/IV}$ oxides.

Additionally, the combined elemental and thermogravimetric results show that the compositions of the oxide materials do not differ greatly: similar amounts of positive ions are required for charge compensation and the relative amount of water intercalated in between the oxide layers is also approximately constant.

SEM images of the oxide particles were taken and clearly showed that the insertion of alkaline and alkaline earth ions has an effect on the morphology of the oxide particles, as they vary in both particle shapes and diameters (see Fig. 2 and ESI†, Figures S4–S7). This is also visible when comparing surface areas determined from gas adsorption experiments (S_{BET} in Table 2) to the EDX data on oxide composition: with the exception of **4** *vs.* **5**, the incorporation of larger amounts of a divalent cation into the structure results in a surface enlargement. Thus **3** (0.27 Ca^{2+} per Mn) has a larger S_{BET} than the corresponding **2** with half as much incorporated calcium (Table 2). Similarly, S_{BET}(**7**) is larger than S_{BET}(**6**) for the Mg-birnessites.

The interlayer distances of oxides **1**, **2**, **4**, **6** and **7** could be determined from X-ray powder diffraction patterns where values of ~7 Å were found as expected for birnessites (Table 2 and, Fig. 3).[54,58] For compounds **3** and **5**, a signal in the 2θ = 10–15°

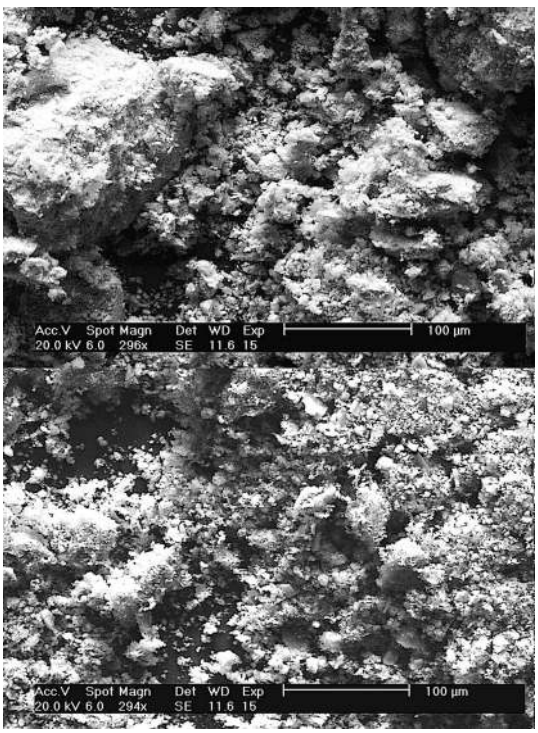

Fig. 2 SEM images of the synthesised $Ca_{0.14}$- (**2**, top) and $Ca_{0.27}$-birnessites (**3**, bottom) illustrating the effect of the insertion of alkaline earth ions on the morphology of the oxide particles. When larger amounts of alkaline earth cations are incorporated into the manganese oxides, smaller particles are formed. See also ESI† Figures S4–S7 for SEM images of other synthetic oxides.

Table 2 Characteristics of the synthesised M-birnessites **1–7**

Compound	Surface area/ $m^2\ g^{-1}$ [a]	Interlayer distance/ Å [b]	Mean Mn oxidation state [c]	Catalytic activity/mmol(O_2) mol(Mn)$^{-1}$ h^{-1} [d]
$K_{0.31}$ (**1**)	55	7.1	3.6	450
$Ca_{0.14}$ (**2**)	95	7.1	3.5	1120
$Ca_{0.27}$ (**3**)	230	—	3.8	860
$Sr_{0.18}$ (**4**)	105	7.0	3.6	720
$Sr_{0.27}$ (**5**)	70	—	3.6	570
$Mg_{0.13}$ (**6**)	75	7.2	3.5	260
$Mg_{0.28}$ (**7**)	130	7.4	3.8	210

[a] Numbers given in the table are rounded S_{BET} values obtained from nitrogen adsorption/desorption curves. [b] Interlayer distances were determined by XRD. For **3** and **5**, the 001 reflection, which is characteristic for the interlayer distance, is absent. [c] Mean Mn oxidation states as determined by XANES. [d] Catalytic activities from water-oxidation catalysis experiments using Ce^{IV} as oxidant.

region characterising the interlayer spacing could be found in the diffraction data of these very amorphous materials. Similar to the influence of the ion content on the morphology of the oxide particles, the increase of alkaline earth metal concentration is also accompanied by the formation of much less ordered

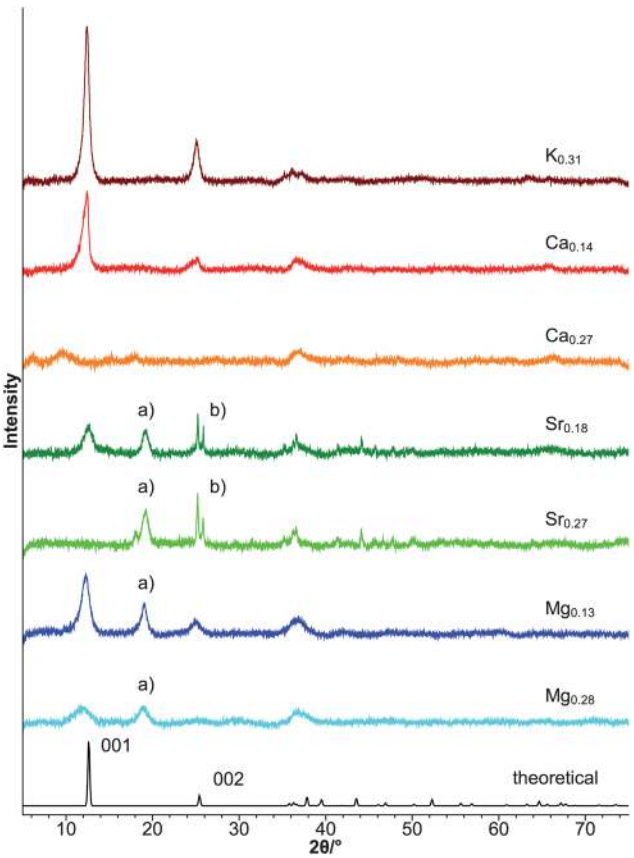

Fig. 3 Powder XRD patterns of birnessites **1–7** and the calculated Bragg reflections[58] for a perfectly ordered Mg-birnessite structure. Reflection a) is not present in pure birnessites, but can be assigned to pyrochroite and ranceite,[59,60] which are intermediates in birnessite synthesis.[60] The pair of reflections at b) have previously been observed for barium manganese oxides[61,62] prepared from the reaction of $Ba(OH)_2$ with $KMnO_4$.[62,63]

birnessites as indicated by the low signal-to-noise ratio of the XRD patterns for oxides **3**, **5** and **7** (Fig. 3). Furthermore, XRD patterns for oxides **4–7** show additional Bragg reflections which are not expected for birnessites. They can be tentatively assigned to the manganese oxide phases pyrochroite and ranceite,[59,60] which have been reported to form as intermediates in the synthesis of M-birnessites (a, Fig. 3).[60] In addition, the XRD patterns of Sr-birnessites **4** and **5** are showing sharp signals in the $2\theta \sim 25°$ section. A similar pair of reflections was previously found for Ba-manganese-oxides[61,62] prepared from reactions of hot $Ba(OH)_2$ with $KMnO_4$.[62,63] Here, the detected pair of reflections may indicate the formation of a structurally related strontium-manganese-oxide phase.

We also recorded infrared spectra of **1–7** (ESI†, Figure S8), which show the expected features for phyllomanganates: relatively high contents of bound water, the presence of OH-groups, and bands that can be assigned to Mn–O vibrations.[64]

XAS experiments

Due to the amorphous character of the prepared powders, a detailed structural analysis of the oxides by X-ray diffraction is not feasible. Therefore we carried out X-ray absorption (XAS) experiments at the Mn K-edge to elucidate the manganese binding motifs. We have already successfully used XAS in a previous study[45] to characterise the structures of synthetic MnCa oxides with catalytic activity in water-oxidation.

X-ray absorption near-edge structure (XANES) spectra of the synthetic Mn oxides are presented in Fig. 4A together with the XANES spectra of Mn oxides of known Mn oxidation states (black lines) serving as reference compounds. The energy position of the absorption edge rise is indicative for the mean oxidation state of the probed element.[65,66] The Mn oxidation state can be estimated from the XANES data by a calculation of the characteristic edge-position energy and a following comparison to reference compounds as described in ref.67 For the average oxidation states of compounds **1–7**, we obtained values between 3.5 and 3.8 in this way (Table 2). This means that the major fraction of the Mn ions of the materials are Mn^{IV} ions. Additionally, smaller fractions of the Mn ions have to be present in the lower manganese oxidation states Mn^{III} or Mn^{II} found in manganese oxides.[57] As only an average oxidation state can be estimated, we cannot determine the relative fractions of Mn^{III} and Mn^{II} ions in the synthetic oxides. The smooth, featureless edge-rises in the XANES spectra of the materials (Fig. 4A) have been previously assigned to Mn oxides with layered structures.[68] This corroborates a birnessite-like structure of the materials (Fig. 5) in agreement with the XRD data presented above, our previous analyses[45] and also the extended X-ray absorption (EXAFS) spectra presented in the following.

Each peak in the Fourier-transformed (FT) EXAFS spectra (Fig. 4B) originates from atoms of oxygen, manganese or alkaline earth metal cations in the vicinity of the X-ray absorbing Mn ion. The peak positions correspond to the distances of the Mn centres to these backscattering atoms. In the Fourier transform, distances are underestimated by 0.3–0.4 Å,[65] but correct distances and coordination numbers can be obtained at high precision from simulations of the EXAFS data (see ESI† for simulation details).

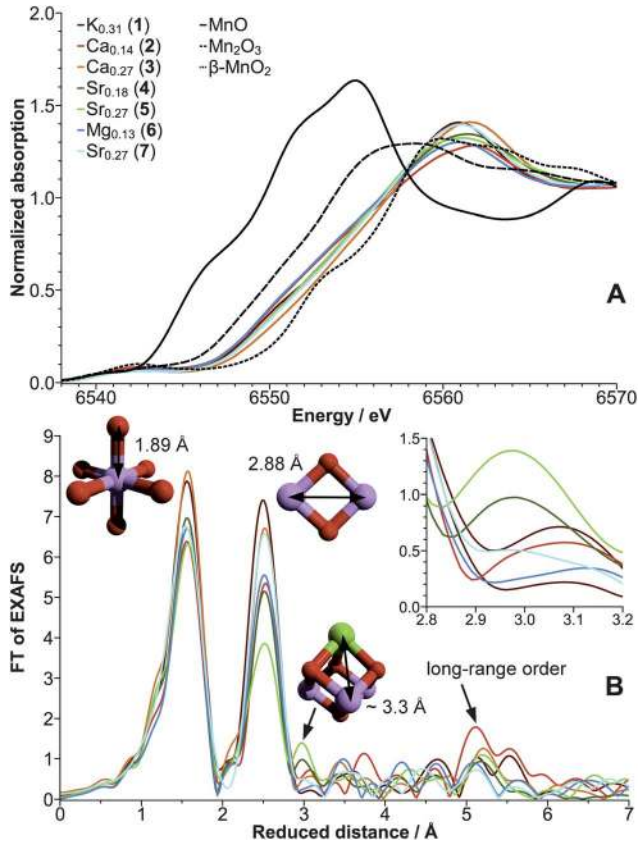

Fig. 4 (A) XANES spectra of **1–7** (coloured lines) and Mn oxides used as reference compounds (black lines). Smooth featureless edge rises and low pre-edge intensities are typical for birnessite-type Mn oxides. The edge-rise energies are indicative for Mn oxidation states between 3.5 and 3.8. (B) Fourier-transformed EXAFS spectra of compounds **1–7**. Each peak relates to a specific structural motif that is schematically depicted (O in red, Mn in purple, alkaline earth metal in green). The region of reduced distances between 2.8 and 3.2 Å, where cubane-like $MMn_{2/3}O_4$ motifs could contribute to the spectra, is shown enlarged in the inset.

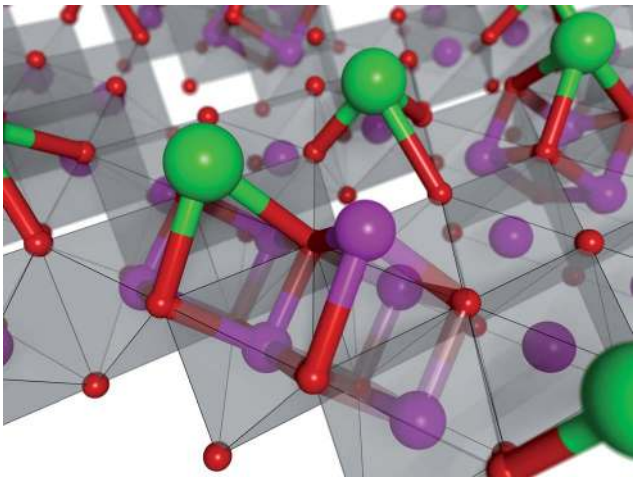

Fig. 5 Structural model for a section of a single layer of an alkaline earth metal birnessite. The layer consists of edge-sharing MnO_6 octahedra with a high number of defects (octahedra in grey, Mn in purple, M^{2+} in green, O in red). M^{2+} ions form corners of $MMn_{2/3}(\mu\text{-}O)_4$ cubes or are placed on top of vacancies of the manganate layers. Additionally, $Mn^{II/III}$ ions in the interlayer space could form the corners of $Mn_4(\mu\text{-}O)_4$ cubes. If such moieties were close to $CaMn_3(\mu\text{-}O)_4$ cubes, a $CaMn_4(\mu\text{-}O)_5$ motif as shown in the foreground would be formed, closely resembling the inorganic core of the OEC of oxygenic photosynthesis. The graphic is based on an layer of ideal MnO_6 octahedra.

Our simulation results for the EXAFS spectra shown in Fig. 4B confirm the presence of layered oxide structures for all synthesised compounds (**1–7**, see Fig. 5 for a model of the oxide layer). The first peak of the EXAFS spectra corresponds to the octahedral ligand sphere of oxygen atoms coordinated to the Mn ions (see ESI†, Tables S3 and S4). Most of the Mn–O distances are found to be close to 1.9 Å, which is a typical value for $Mn^{IV}O_6$ octahedra present for example in the reference material β-MnO_2.[69] The fact that about 20% of the Mn–O distances are significantly longer (~2.3 Å) indicates contributions of either Mn^{III} (as *e.g.* in α-$Mn^{III}_2O_3$[70] with two elongated Mn–O distances due to the Jahn–Teller distortion of the d^4 ions) or Mn^{II} ions (as in $Mn^{II}O$).[71] In accordance with the XANES analysis, the oxides with lower Mn oxidation states (**2**, **4**, **5** and **6**, see Table 2) also have a higher content of these longer Mn–O distances originating from Mn^{III} or Mn^{II}.

The second prominent FT peak found at reduced distances of ~2.5 Å is typical for di-μ-oxido connected Mn ions. This is the dominating bridging motif in layered Mn oxides. From our simulations, a Mn–Mn distance of ~2.88 Å can be determined, as typically found in layered Mn oxides.[72] However, the relatively high Debye–Waller parameters (see ESI†) indicate a high heterogeneity for this shell, which could result from the presence of Mn^{III} ions in the MnO_6-layers, which has been observed for synthetic triclinic birnessite minerals.[73] This heterogeneity should decrease the peak amplitude at ~2.5 Å and it is indeed lower for compounds **2**, **4**, **5** and **6** for which the fraction of Mn^{III} ions is estimated to be higher compared to **3** and **7** (Table 2, see ESI, Figure S3†).

The presence of an FT peak at a reduced distance of around 3 Å is predicted for cubane-like metal-oxido motifs.[45,74] Such a peak is most clearly visible in the Sr-containing oxides (see inset in Fig. 4B). By simulations, we determined a Mn–Sr distance of 3.3 Å and the EXAFS coordination number suggests the presence of about 0.5 Sr^{2+} ions per X-ray absorbing Mn ion. The same $M^{2+}Mn_3(\mu\text{-}O)_4$ motif is thus possibly present also in the Ca-containing samples **2** and **3**, but here it cannot be resolved reliably.

The extent of long-range order in the layer fragments can be estimated from the magnitude of FT peaks at longer distances. A distance of about 5.8 Å (equal to two Mn–Mn distances of 2.88 Å) corresponds to three collinearly arranged Mn ions interconnected by di-μ-oxido bridges. The amplitude of the corresponding FT peak reflects the extent of long-range order in the oxide[75] but in the present investigations, the low peak amplitude rendered a quantification of this signal by EXAFS simulation unreliable. Instead we used the EXAFS corresponding to an FT peak at about 5.1 Å for assessment of the long-range order in the oxides. Comparing the two M^{2+} : Mn stoichiometries for each alkaline earth metal (see Table 1), we find that higher M^{2+} concentrations promote more extensive disorder, in agreement with the lack of 001 XRD reflections detected for compounds **3** and **5** (see Fig. 3).

Oxygen evolution experiments

Water-oxidation experiments were carried out to investigate the catalytic activities of the synthetic K-, Ca-, Sr- and Mg-birnessites **1–7**. In these experiments, Ce^{IV} was used as oxidant. Firstly, the high oxidation potential of the Ce^{IV}/Ce^{III} couple ($E_0 \sim +1.4$ V *vs.* NHE) is suitable for the water-oxidation reaction. Additionally, Ce^{IV} is acting as a single-electron oxidant, a central requirement for model reactions to mimic the fourfold one-electron chemistry of natural water-oxidation. Importantly, it has also been shown by ^{18}O-labelling experiments, that oxygen evolution reactions where Ce^{IV} is used as an oxidant and manganese oxides as catalysts are "real" water-oxidation processes, meaning that both oxygen atoms of the formed O_2 originate from the bulk water.[76] In contrast, if oxygen transferring reagents like oxone (HSO_5^-) are used, it has been found that at least one oxygen atom of the formed O_2 is originating from the oxidant.

In our experiments, oxides **1–7** were suspended in 0.25 M solutions of Ce^{IV} in closed septum vials. The progress of the reaction was subsequently analysed by headspace gas chromatography to detect the O_2 product (Fig. 6, see ESI† for details). Even as we were able to characterise the structure of the oxide materials, the catalytically active units are currently unknown. Hence, oxygen evolution rates were calculated per manganese ion as Mn is definitely involved in the reaction steps of the catalytic process. To assure that oxygen evolution does not merely result from dissolving the Mn-oxides at the low pH of the catalytic mixture, reference experiments were carried out using HNO_3 at pH $\sim$ 2. Here, no oxygen evolution could be detected (Fig. 6, black trace).

All synthetic K-, Ca-, Sr- and Mg-birnessites show catalytic activity in water-oxidation experiments using Ce^{IV} (Fig. 6, Table 2). On a per manganese basis, catalysis proceeds with the formation of only 0.2–1.2 molecules of O_2 per manganese ion and hour (and thus is by about a factor of 10^6 (!) slower than in PSII).[8] However, one should keep in mind the fact that in our experiments random diffusion-controlled redox processes occur between Ce^{IV}-ions and birnessite particles while PSII contains an amazingly optimized and elaborate electron-transfer chain.[4,18–20,25,77] Therefore, absolute turnover frequencies between the natural enzyme and our synthetic inorganic system can hardly be compared.

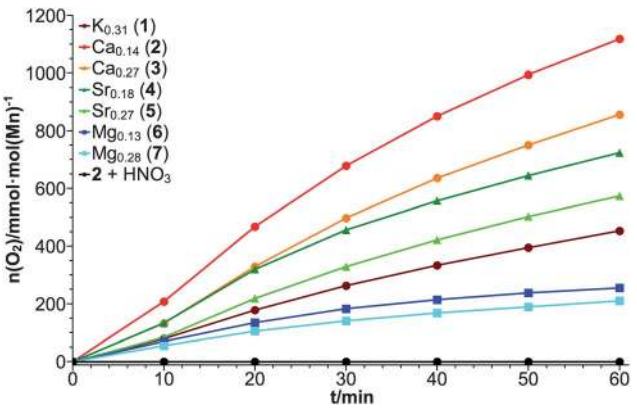

Fig. 6 Traces for O_2 evolution from experiments on water-oxidation-catalysis by different M-birnessites. Oxides **1–7** (1 mg mL^{-1}) were suspended in solutions of Ce^{IV} (0.25 M) and filled into septum vials. The progress of the reaction was then analysed by headspace gas chromatography to detect and quantify the O_2 product. No oxygen evolution could be detected for suspensions of oxides **1–7** in HNO_3 (pH $\sim$ 1.7), as shown for **2** + HNO_3 as an example (black trace).

But interestingly, when considering relative rates, we find marked differences in oxygen-evolution catalysis. Depending on the type and the concentration of the alkaline earth cations, reaction rates differ in a fashion resembling catalytic trends found for the native PSII enzyme. Overall, the Ca-birnessites **2** and **3** are showing the highest activity in catalysis (Fig. 6, Table 2). Oxygen evolution rates for Sr-birnessites are lower, but still high in comparison to the rates for the Mg-birnessites **6** and **7** which are only showing modest activity. The catalytic activity of **1**, the reference material virtually free of alkaline earth ions, is in between those observed for the Sr- and Mg-birnessites.

In short, the trend in activity for M-birnessites as water-oxidation catalysts in dependence of the type of intercalated alkaline earth cation can be formulated as $Ca^{2+} > Sr^{2+} > K^+ > Mg^{2+}$. For the pairs of Ca-(**2**,**3**), Sr-(**4**,**5**) and Mg-(**6**,**7**) birnessites, the catalytic activity decreases for each pair if the concentrations of alkaline earth cations in the oxides is increased. We analysed the data for other possible correlations, but found no convincing trends (see ESI†, Figures S12–S16, where comparisons of activity *vs.* surface area, activity *vs.* alkaline earth concentrations, activity *vs.* total alkali/alkaline earth concentration, activity *vs.* additional positive charges and activity *vs.* mean Mn oxidation state are plotted).

We thus conclude that the major parameter influencing catalytic activity is the nature of the secondary cation followed as a second factor by the concentration of these additional cations in the material. Furthermore, it can be seen in Fig. 6 that the observed oxygen-evolution rates decrease slightly over the 60 min. period the catalyses were monitored. We found before that Ca is partially (<10% of total amount) removed from the birnessite structures under our reaction conditions,[44] which might explain the observed slower catalysis. Najafpour *et al.* recently showed that the treatment of Ca-manganese-oxides with $CaCl_2$ solution after experiments for water-oxidation results in the restoration of the catalytic activity for the materials.[78] Thus, to enhance long-term stability, the use of calcium containing buffers in future water-oxidation experiments appears to be a promising approach. Furthermore, we see great potential to improve the catalytic performances of the oxides by further variations of their compositions, their morphologies and the development of better electron-transfer-chains connecting catalysts and oxidation agents. Especially for applications in artificial photosynthesis, the coupling of water-oxidation-catalysis by birnessites to light-driven charge separation is essential and should be a focus of future efforts.

As mentioned above, a major motivation for the syntheses of the alkaline earth birnessites was their potential model character for the known Ca^{2+} substitution effects observed for PSII. In two previously reported independent sets of experiments with the photoenzyme, Ca^{2+} was removed from isolated PSII resulting in a more or less complete loss of activity for water-oxidation.[31,33] The subsequent addition of Ca^{2+} to the depleted enzyme restored catalytic activity to a large degree, while the addition of Mg^{2+} had

no effect and left the enzyme at the residual activity of ~10% observed after Ca^{2+}-removal. However, enzyme activity could also be regained by the addition of Sr^{2+}, but only at decreased oxygen evolution rates when compared to the recovery by Ca^{2+} addition.[31,33] Thus, the trend for the ability of these cations to restore water-oxidation activity for Ca^{2+}-depleted PSII can be formulated as $Ca^{2+} > Sr^{2+} \gg Mg^{2+} \sim Na^{+}$ and is therefore virtually identical to the results of our activity study on synthetic birnessites presented above.

For a better comparison of the influence of the alkaline earth cations on catalysis, Fig. 7 shows the relative oxygen-evolution rates for the M-birnessites **1**, **2**, **4** and **6** (brown bars, activity of the $Ca_{0.14}$-birnessite **2** was set to 100%) and for Ca^{2+}, Sr^{2+}, Mg^{2+} and Na^{+}-reactivated PSII (green bars, activity of Ca^{2+} reactivated PSII was set to 100%). Two reported datasets[31,33] for the enzyme are shown. It has to be noted that the catalytic activities observed for Ca^{2+}-depleted and for Mg^{2+} exchanged PSII could originate from a small number of enzymes for which Ca^{2+}-removal was incomplete.[33]

It is clearly visible in Fig. 7 that the differences of relative oxygen evolution rates show striking similarities between the synthetic birnessites and the PSII enzyme. Both the general reactivity trends as well as the quantitative comparisons are rather consistent. Of course, it cannot be ignored that there are also differences between the datasets. It seems that PSII reacts in a more pronounced way to cation exchange than the synthetic oxides. So, the removal of Ca^{2+} or substitution with Mg^{2+} or alkali metal ions results in nearly complete inactivation.[33,79] In contrast, all birnessites presented here are at least moderately active water-oxidation catalysts. This is no surprise, as even "Mn-only" oxides like Mn_2O_3 or colloidal MnO_2 are active in water-oxidation-catalysis,[80,81] but only at much lower rates than birnessites.[44] (For electrochemical water oxidation by a new electrodeposited Mn-only oxide, see ref.82.) Nevertheless, the results indicate possible similarities in the function of the alkaline earth cations and thus also in the water-oxidation mechanism for both M-birnessites and the OEC, as will be discussed in the following section.

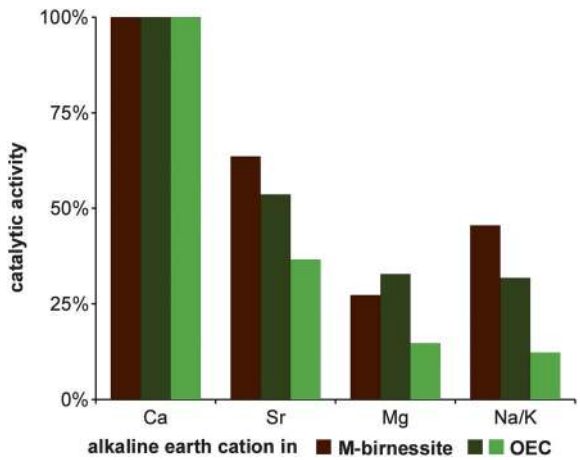

Fig. 7 Relative catalytic activities of M^{2+}-birnessites **2**, **4**, **6** and K-birnessite **1** respectively (brown, activity of $Ca_{0.14}$-birnessite **2** was set to 100%) in comparison to Ca^{2+}-depleted PSII reactivated with Ca^{2+}, Sr^{2+}, Mg^{2+} or Na^{+} solutions (dark green[31] and light green,[33] activity of Ca-reactivated PSII was set to 100%).

Hypotheses on the role of Ca^{2+} for O–O bond formation

With respect to water-oxidation catalysed by the OEC, various mechanisms for the O–O bond formation step have been postulated. In many scenarios, bridging oxido (μ-O^{2-}) or terminal oxyl ($O^{\bullet -}$) groups, as well as hydroxide or water molecules in the vicinity of the OEC are considered to be important for the pathways leading towards the transition-state.[8,18,83] Interestingly, the structural motifs necessary for these reaction pathways can also be found in layered manganese oxides.[44,45] Moreover, we now find OEC-like trends concerning the importance of the secondary cations for catalytic activities. Therefore we propose that mechanistic concepts for O–O bond formation developed for the OEC may be adopted to the catalytic action by M-birnessites as well, so that the role of Ca^{2+} could be an activation of terminal or bridging oxygen atoms for the O–O bond formation step. To illustrate this potential catalytic role of calcium, adaptations of published mechanistic proposals for the OEC to the Ca-birnessite structure are shown in Fig. 8. As presented in this graphic, Ca^{2+} could act as a potential binding and activation site for substrate water in the form of hydroxide[39] (route a), or water directly.[8,18,84–86] Alternatively, oxyl- or oxido ligands could be activated to form a peroxide intermediate from either two bridging oxido-ligands[87,88] (route e), possibly activated by Ca^{2+} (route b), a μ_2- and a μ_3-O^{2-}, both bound to calcium[30] (route c) or a μ_3-oxido- and a terminal oxyl-ligand[89] (route d). Moreover, other mechanisms have been suggested which do not involve calcium but an outer-sphere water (or hydroxide) that reacts directly with manganese-bound oxygen atoms (route f).[27,90,91] Our results indicate that such Mn-only routes (e and f) may be less important, but on the basis of our data none of the mechanisms presented in Fig. 8 can be ruled out at this point.

In addition to O–O bond formation, proton management is essential for the efficient catalysis of water-oxidation.[92,93] Oxido or hydroxido bridges of the OEC have been proposed to be involved in proton-coupled electron transfer (PCET) during the accumulation of redox equivalents and possibly also in the O–O bond formation step itself.[8,29,94] Beyond doubt, the protein matrix is also involved in proton abstraction and transfer in biological water oxidation.[8,25,29,95,96] In the M-birnessites, proton management by organic residues is not possible, but the oxido bridges present in M-birnessites could be involved in proton abstraction from substrate water molecules. In addition, the deprotonation of hydroxido bridges may play a key role for the necessary charge-compensation to accumulate several oxidizing equivalents before O–O bond formation can occur.[8] Oxido bridges also may substitute for the protein matrix of PSII by facilitating multi-step long-distance proton transfer within and at the surface of the birnessite particles.

Conclusion and outlook

In summary, we synthesised and characterised various layered K-, Ca-, Sr- and Mg-containing manganese oxides that differ in their elemental compositions and morphologies. We were able to show that these mixed manganese oxides feature an amorphous birnessite type structure, namely layers of edge-sharing MnO_6-octahedra with a large number of defects and additional cations

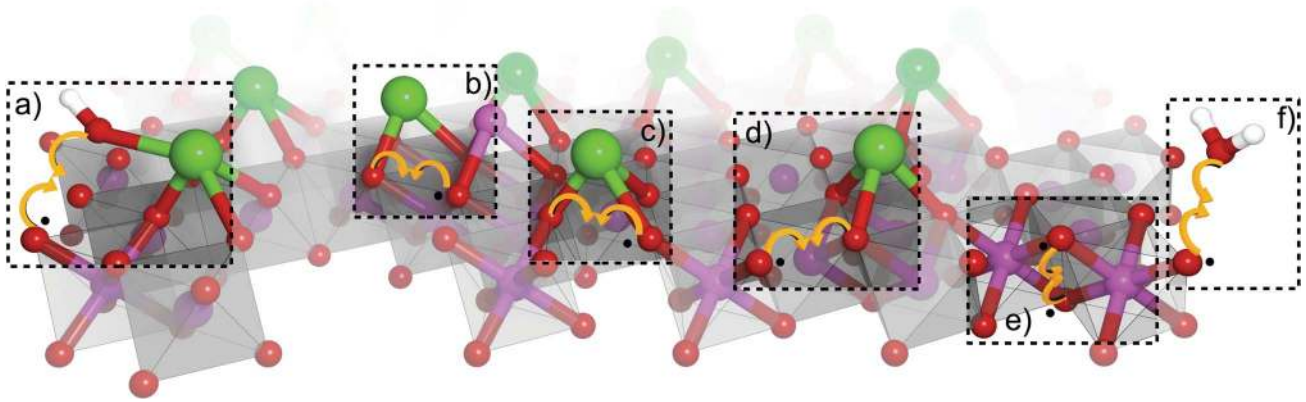

Fig. 8 Possible routes for O–O bond formation in water-oxidation catalysed by M-birnessites in analogy to dioxygen formation routes suggested for the OEC (colour code as in Fig. 2). a) Ca (or Sr respectively) is acting as binding and activation site for a nucleophilic attack by hydroxide. The O–O bond formation takes place by coupling to a terminal oxyl radical. Terminal or bridging oxygens are also discussed to be involved in other scenarios for O–O coupling, where always one oxygen might be present as an oxyl radical, $O^{\bullet -}$. Here, the O–O bond might form between two bridging oxygens, activated by Ca (b), a μ_2- and a μ_3-O^{2-}, both bound to Ca (c), one terminal and one μ_3-oxygen (d), or between two μ_2-oxygen atoms of the oxide layer (e). Furthermore, a mechanism where water is directly coupled to a terminal oxyl radical (f) might be of importance.

intercalated in between the layers of the phyllomanganates. XANES and EXAFS spectra at the Mn K-edge were recorded to elucidate structural details. Structural motifs analogous to previously studied birnessite catalysts[45] have been found, as Ca^{2+}, Sr^{2+} and Mg^{2+} ions form edges of open (incomplete) or closed (complete) $CaMn_{2/3}(\mu\text{-}O)_4$, $SrMn_{2/3}(\mu\text{-}O)_4$ and $MgMn_{2/3}(\mu\text{-}O)_4$ cubes respectively. They are also found above vacancies in the MnO_6-layer. Furthermore, $Mn^{II/III}$ ions could be present in the interlayer space, possibly forming $Mn_4(\mu\text{-}O)_4$ cubes.

Experiments on water-oxidation catalysis show clear differences in the reactivity for the synthetic M-birnessites depending on the type of intercalated alkaline earth cation. A catalytic activity trend $Ca^{2+} > Sr^{2+} > Mg^{2+}$ can be formulated. Strikingly, this series corresponds to the order of oxygen-evolution rates observed for the natural PSII enzyme and its Sr^{2+} and Mg^{2+} substituted forms. Thus, we suggest that Ca^{2+} could have a similar function in catalysis for both systems. Related O–O bond formation mechanisms involving calcium *and* manganese (Fig. 8, b–d) may be effective both in the biological PSII and in the synthetic birnessites. This proposal is also supported by the presence of structural motifs within the layers of M-birnessites which are also discussed in photosynthetic water-oxidation, namely di-μ-oxido-bridged $Mn^{III/IV}$ ions, μ-oxido-bridging between Mn and Ca ions, as well as terminal water (or hydroxido) ligands of Ca^{2+}.

In conclusion, our findings presented here show that M-birnessites are outstanding OEC model compounds as they appear to mimic not only the structure and function of the OEC, but also the essential role of the Ca^{2+} cation to achieve maximum catalytic rates. Furthermore, if manganese oxides are to be used as catalysts for artificial photosynthesis, the best choice known to date seems to be water-oxidation catalysis by calcium birnessites.

Experimental

M-birnessites were synthesised following a route published by Luo *et al.*[55] using comproportionation reactions of Mn^{2+} and MnO_4^- in the presence of Ca^{2+}, Sr^{2+} and Mg^{2+}, respectively, under alkaline conditions.

The XAS measurements were performed at the Helmholtz-Zentrum Berlin für Materialien und Energie (formerly BESSY II, Berlin). The measurements at the manganese K-edge were acquired in transmission mode at the KMC-1 bending-magnet beamline at 20 K in a cryostat (Oxford-Danfysik) with a liquid-helium flow system.

All details concerning syntheses, characterisation methods, XAS measurements, EXAFS simulations and experiments on water-oxidation catalysis are given in the ESI†.

Acknowledgements

This work was generously supported by the Fonds der Chemischen Industrie (Liebig fellowship of Ph.K.) and the Deutsche Forschungsgemeinschaft (DFG). We thank M. Mertin and Dr F. Schäfers for their excellent technical support at the beamline KMC-1 of BESSY, a synchrotron radiation source in Berlin operated by the Helmholtz-Zentrum Berlin. Furthermore, financial support by the Berlin cluster of excellence "Unifying Concepts in Catalysis" (UniCat) and the European Union (7th framework program, SOLAR-H2 consortium, #212508) is gratefully acknowledged.

References

1 M. Kirch, J.-M. Lehn and J.-P. Sauvage, *Helv. Chim. Acta*, 1979, **62**, 1345–1384.
2 N. S. Lewis and D. G. Nocera, *Proc. Natl. Acad. Sci. U. S. A.*, 2006, **103**, 15729–15735.
3 N. Armaroli and V. Balzani, *Angew. Chem., Int. Ed.*, 2007, **46**, 52–66.
4 W. Lubitz, E. J. Reijerse and J. Messinger, *Energy Environ. Sci.*, 2008, **1**, 15–31.
5 V. Balzani, A. Credi and M. Venturi, *ChemSusChem*, 2008, **1**, 26–58.
6 A. Magnuson, M. Anderlund, O. Johansson, P. Lindblad, R. Lomoth, T. Polivka, S. Ott, K. Stensjö, S. Styring, V. Sundström and L. Hammarström, *Acc. Chem. Res.*, 2009, **42**, 1899–1909.
7 K. Maeda and K. Domen, *J. Phys. Chem. Lett.*, 2010, **1**, 2655–2661.
8 H. Dau, C. Limberg, T. Reier, M. Risch, S. Roggan and P. Strasser, *ChemCatChem*, 2010, **2**, 724–761.

9 M. Wiechen, H.-M. Berends and P. Kurz, *Dalton Trans.*, 2012, **41**, 21–31.
10 L. Duan, L. Tong, Y. Xu and L. Sun, *Energy Environ. Sci.*, 2011, **4**, 3296–3313.
11 H. Yamazaki, A. Shouji, M. Kajita and M. Yagi, *Coord. Chem. Rev.*, 2010, **254**, 2483–2491.
12 L. Duan, F. Bozoglian, S. Mandal, B. Stewart, T. Privalov, A. Llobet and L. Sun, *Nat. Chem.*, 2012, **4**, 418–423.
13 M. W. Kanan and D. G. Nocera, *Science*, 2008, **321**, 1072–1075.
14 J. J. Concepcion, M.-K. Tsai, J. T. Muckerman and T. J. Meyer, *J. Am. Chem. Soc.*, 2010, **132**, 1545–1557.
15 S. Romain, L. Vigara and A. Llobet, *Acc. Chem. Res.*, 2009, **42**, 1944–1953.
16 J. K. Hurst, *Coord. Chem. Rev.*, 2005, **249**, 313–328.
17 A. Sartorel, P. Miro, E. Salvadori, S. Romain, M. Carraro, G. Scorrano, M. D. Valentin, A. Llobet, C. Bo and M. Bonchio, *J. Am. Chem. Soc.*, 2009, **131**, 16051–16053.
18 J. P. McEvoy and G. W. Brudvig, *Chem. Rev.*, 2006, **106**, 4455–4483.
19 J. Yano, J. Kern, K. Sauer, M. J. Latimer, Y. Pushkar, J. Biesiadka, B. Loll, W. Saenger, J. Messinger, A. Zouni and V. K. Yachandra, *Science*, 2006, **314**, 821–825.
20 H. Dau, I. Zaharieva and M. Haumann, *Curr. Opin. Chem. Biol.*, 2012, **16**, 3–10.
21 Y. Gorlin and T. F. Jaramillo, *J. Am. Chem. Soc.*, 2010, **132**, 13612–13614.
22 F. Jiao and H. Frei, *Energy Environ. Sci.*, 2010, **3**, 1018–1027.
23 E. A. Karlsson, B.-L. Lee, T. Åkermark, E. V. Johnston, M. D. Kärkäs, J. Sun, Ö. Hansson, J.-E. Bäckvall and B. Åkermark, *Angew. Chem., Int. Ed.*, 2011, **50**, 11715–11718.
24 K. Maeda, A. Xiong, T. Yoshinaga, T. Ikeda, N. Sakamoto, T. Hisatomi, M. Takashima, D. Lu, M. Kanehara, T. Setoyama, T. Teranishi and K. Domen, *Angew. Chem., Int. Ed.*, 2010, **49**, 4096–4099.
25 Y. Umena, K. Kawakami, J.-R. Shen and N. Kamiya, *Nature*, 2011, **473**, 55–60.
26 B. Kok, B. Forbush and M. McGloin, *Photochem. Photobiol.*, 1970, **11**, 457–475.
27 H. Dau, L. Iuzzolino and J. Dittmer, *Biochim. Biophys. Acta, Bioenerg.*, 2001, **1503**, 24–39.
28 M. Haumann, C. Müller, P. Liebisch, L. Iuzzolino, J. Dittmer, M. Grabolle, T. Neisius, W. Meyer-Klaucke and H. Dau, *Biochemistry*, 2005, **44**, 1894–1908.
29 H. Dau and M. Haumann, *Coord. Chem. Rev.*, 2008, **252**, 273–295.
30 P. E. M. Siegbahn, *Acc. Chem. Res.*, 2009, **42**, 1871–1880.
31 D. F. Ghanotakis, G. T. Babcock and C. F. Yocum, *FEBS Lett.*, 1984, **167**, 127–130.
32 A. Boussac and A. W. Rutherford, *Biochemistry*, 1988, **27**, 3476–3483.
33 T.-A. Ono and Y. Inoue, *FEBS Lett.*, 1988, **227**, 147–152.
34 M. Miyao and N. Murata, *FEBS Lett.*, 1984, **168**, 118–120.
35 A. Boussac, J. L. Zimmermann and A. W. Rutherford, *Biochemistry*, 1989, **28**, 8984–8989.
36 A. Boussac, J.-L. Zimmermann and A. W. Rutherford, *FEBS Lett.*, 1990, **277**, 69–74.
37 A. Boussac, F. Rappaport, P. Carrier, J. M. Verbavatz, R. Gobin, D. Kirilovsky, A. W. Rutherford and M. Sugiura, *J. Biol. Chem.*, 2004, **279**, 22809–22819.
38 N. Cox, L. Rapatskiy, J.-H. Su, D. A. Pantazis, M. Sugiura, L. Kulik, P. Dorlet, A. W. Rutherford, F. Neese, A. Boussac, W. Lubitz and J. Messinger, *J. Am. Chem. Soc.*, 2011, **133**, 3635–3648.
39 V. L. Pecoraro, M. J. Baldwin, M. T. Caudle, W. Y. Hsieh and N. A. Law, *Pure Appl. Chem.*, 1998, **70**, 925–929.
40 J. S. Vrettos, J. Limburg and G. W. Brudvig, *Biochim. Biophys. Acta, Bioenerg.*, 2001, **1503**, 229–245.
41 J. P. McEvoy and G. W. Brudvig, *Phys. Chem. Chem. Phys.*, 2004, **6**, 4754–4763.
42 V. K. Yachandra and J. Yano, *J. Photochem. Photobiol., B*, 2011, **104**, 51–59.
43 C. F. Yocum, *Coord. Chem. Rev.*, 2008, **252**, 296–305.
44 M. M. Najafpour, T. Ehrenberg, M. Wiechen and P. Kurz, *Angew. Chem., Int. Ed.*, 2010, **49**, 2233–2237.
45 I. Zaharieva, M. M. Najafpour, M. Wiechen, M. Haumann, P. Kurz and H. Dau, *EnergyEnviron. Sci.*, 2011, **4**, 2400–2408.
46 R. K. Hocking, R. Brimblecombe, L.-Y. Chang, A. Singh, M. H. Cheah, C. Glover, W. H. Casey and L. Spiccia, *Nat. Chem.*, 2011, **3**, 461–466.
47 B. A. Pinaud, Z. Chen, D. N. Abram and T. F. Jaramillo, *J. Phys. Chem. C*, 2011, **115**, 11830–11838.
48 G. F. Swiegers, J. K. Clegg and R. Stranger, *Chem. Sci.*, 2011, **2**, 2254–2262.
49 M. M. Najafpour, *Chem. Commun.*, 2011, **47**, 11724–11726.
50 M. Risch, V. Khare, I. Zaharieva, L. Gerencser, P. Chernev and H. Dau, *J. Am. Chem. Soc.*, 2009, **131**, 6936–6937.
51 M. W. Kanan, J. Yano, Y. Surendranath, M. Dinca, V. K. Yachandra and D. G. Nocera, *J. Am. Chem. Soc.*, 2010, **132**, 13692–13701.
52 M. Risch, K. Klingan, J. Heidkamp, D. Ehrenberg, P. Chernev, I. Zaharieva and H. Dau, *Chem. Commun.*, 2011, **47**, 11912–11914.
53 M. Dincă, Y. Surendranath and D. G. Nocera, *Proc. Natl. Acad. Sci. U. S. A.*, 2010, **107**, 10337–10341.
54 J. E. Post, *Proc. Natl. Acad. Sci. U. S. A.*, 1999, **96**, 3447–3454.
55 J. Luo, Q. Zhang, A. Huang, O. Giraldo and S. L. Suib, *Inorg. Chem.*, 1999, **38**, 6106–6113.
56 S. M. Webb, B. M. Tebo and J. R. Bargar, *Am. Mineral.*, 2005, **90**, 1342–1357.
57 N. N. Greenwood and A. Earnshaw, *Chemistry of the Elements*, Butterworth-Heinemann, Oxford, 1997.
58 J. E. Post and D. R. Veblen, *Amer. Mineral.*, 1990, **75**, 477–489.
59 O. Bricker, *Amer. Mineral.*, 1965, **50**, 1296–1354.
60 J. Luo, Q. Zhang and S. L. Suib, *Inorg. Chem.*, 2000, **39**, 741–747.
61 J. D. Hanawalt, H. W. Rinn and L. K. Frevel, *Ind. Eng. Chem., Anal. Ed.*, 1938, **10**, 457–512.
62 F. Jellinek, *J. Inorg. Nucl. Chem.*, 1960, **13**, 329–331.
63 H. I. Schlesinger and H. B. Siems, *J. Am. Chem. Soc.*, 1924, **46**, 1965–1978.
64 O. Glemser, G. Gattow and H. Meisiek, *Z. Anorg. Allg. Chem.*, 1961, **309**, 1–19.
65 B. Teo, *EXAFS: Basic principles and data analysis*, Springer Verlag, Berlin, Germany, 1986.
66 L. S. Kau, D. J. Spira-Solomon, J. E. Penner-Hahn, K. O. Hodgson and E. I. Solomon, *J. Am. Chem. Soc.*, 1987, **109**, 6433–6442.
67 H. Dau, P. Liebisch and M. Haumann, *Anal. Bioanal. Chem.*, 2003, **376**, 562–583.
68 A. C. Gaillot, D. Flot, V. A. Drits, A. Manceau, M. Burghammer and B. Lanson, *Chem. Mater.*, 2003, **15**, 4666–4678.
69 R. W. G. Wyckoff, *Crystal Structures 1*, Interscience Publishers, New York, 1963, pp. 239–444.
70 S. Geller, *Acta Crystallogr., Sect. B: Struct. Crystallogr. Cryst. Chem.*, 1971, **27**, 821–828.
71 R. E. Pacalo and E. K. Graham, *Phys. Chem. Miner.*, 1991, **18**, 69–80.
72 M. Villalobos, B. Lanson, A. Manceau, B. Toner and G. Sposito, *Am. Mineral.*, 2006, **91**, 489–502.
73 B. Lanson, V. A. Drits, Q. Feng and A. Manceau, *Amer. Mineral.*, 2002, **87**, 1662–1671.
74 G. C. Dismukes, R. Brimblecombe, G. A. N. Felton, R. S. Pryadun, J. E. Sheats, L. Spiccia and G. F. Swiegers, *Acc. Chem. Res.*, 2009, **42**, 1935–1943.
75 M. Risch, K. Klingan, F. Ringleb, P. Chernev, I. Zaharieva, A. Fischer and H. Dau, *ChemSusChem*, 2012, **5**, 542–549.
76 D. Shevela, S. Koroidov, M. M. Najafpour, J. Messinger and P. Kurz, *Chem.–Eur. J.*, 2011, **17**, 5415–5423.
77 A. Grundmeier and H. Dau, *Biochim. Biophys. Acta, Bioenerg.*, 2012, **1817**, 88–105.
78 M. M. Najafpour, S. Nayeri and B. Pashaei, *Dalton Trans.*, 2011, **40**, 9374–9378.
79 T. Ono, A. Rompel, H. Mino and N. Chiba, *Biophys. J.*, 2001, **81**, 1831–1840.
80 A. Harriman, I. J. Pickering, J. M. Thomas and P. A. Christensen, *J. Chem. Soc., Faraday Trans. 1*, 1988, **84**, 2795–2806.
81 V. Y. Shafirovich, N. K. Khannanov and A. E. Shilov, *J. Inorg. Biochem.*, 1981, **15**, 113–129.
82 I. Zaharieva, P. Chernev, M. Risch, K. Klingan, M. Kohlhoff, A. Fischer and H. Dau, *Energy Environ. Sci.*, DOI: 10.1039/C2EE21191B.
83 C. W. Cady, R. H. Crabtree and G. W. Brudvig, *Coord. Chem. Rev.*, 2008, **252**, 444–455.
84 J. S. Vrettos, J. Limburg and G. W. Brudvig, *Biochim. Biophys. Acta, Bioenerg.*, 2001, **1503**, 229–245.
85 J. P. McEvoy, J. A. Gascon, V. S. Batista and G. W. Brudvig, *Photochem. Photobiol. Sci.*, 2005, **4**, 940–949.
86 K. N. Ferreira, T. M. Iverson, K. Maghlaoui, J. Barber and S. Iwata, *Science*, 2004, **303**, 1831–1838.

87 V. K. Yachandra, K. Sauer and M. P. Klein, *Chem. Rev.*, 1996, **96**, 2927–2950.
88 W. Ruettinger, M. Yagi, K. Wolf, S. Bernasek and G. C. Dismukes, *J. Am. Chem. Soc.*, 2000, **122**, 10353–10357.
89 J. Messinger, *Phys. Chem. Chem. Phys.*, 2004, **6**, 4764–4771.
90 J. Messinger, M. Badger and T. Wydrzynski, *Proc. Natl. Acad. Sci. U. S. A.*, 1995, **92**, 3209–3213.
91 W. Hillier and T. Wydrzynski, *Biochim. Biophys. Acta, Bioenerg.*, 2001, **1503**, 197–209.
92 H. Dau and M. Haumann, *Science*, 2006, **312**, 1471–1472.
93 H. Dau and M. Haumann, *Biochim. Biophys. Acta, Bioenerg.*, 2007, **1767**, 472–483.
94 H. Dau and M. Haumann, *Photosynth. Res.*, 2005, **84**, 325–331.
95 J. W. Murray and J. Barber, *J.Struct. Biol.*, 2007, **159**, 228–237.
96 F. Ho, *Photosynth. Res.*, 2008, **98**, 503–522.